Effect of mechanical activation on carbothermic reduction and nitridation of titanomagnetite concentrates

Xiaojin Wen, Wen Yu, Danliang Zeng, LiangLiang Zhu, Jiangan Chen

Faculty of Resource and Environmental Engineering, Jiangxi University of Science and Technology, Ganzhou 341000, China

Corresponding author: yuwenminer@163.com (Wen Yu)

Abstract: The carbothermic reduction and nitridation process of titanomagnetite concentrates with the help of mechanical activation were investigated by particle size analysis, thermodynamic calculation, thermogravimetric analysis, X-ray diffraction analysis, scanning electron microscopy, and energy-dispersive spectroscopy analysis. The thermogravimetric and X-ray diffraction results indicated that either the reduction of iron oxide or the reduction and nitridation of M_3O_5 to TiN could be promoted significantly with the increase in activation time. The results obtained from scanning electron microscopy and energy-dispersive spectroscopy showed that, when samples were not activated, chunks of and thin M_3O_5 were derived from the reduction of ilmenite and titanomagnetite. They were severely sintered with impurities to form a dense structure. As a result, M_3O_5 was difficult to be converted to TiN, especially chunks of M_3O_5. However, when samples were activated, the sintering degrees of the impurity and M_3O_5 were mitigated, and the particle size of the iron as a medium for delivering C to M_3O_5 was decreased in the roasted product. This condition enhanced the diffusion of C to the surface of M_3O_5. Meanwhile, the bulk of ilmenite was broken in the activation process, which prevented the formation of chunks of M_3O_5. Thus, the conversion of M_3O_5 to TiN was promoted.

Keywords: titanomagnetite concentrates, carbothermic reduction, mechanical activation, titanium nitride

1. Introduction

Titanomagnetite is an important resource for the metallurgical industry because it contains iron, titanium, and vanadium (Paunova, 2002a). Reports indicate that it is widely distributed in China, Russia, South Africa, and New Zealand (Li et al., 2017). In China, titanomagnetite reserves are more than 18 billion tons and are mainly distributed in Panzhihua, Sichuan Province (Hu et al., 2013; Zhao et al., 2019). At present, the blast furnace process is always used to recover Fe and V from TMC. Moreover, nearly all of the Ti remains in the slag, which forms a titanium-bearing slag with the variation in the content of TiO_2 from 22% to 25% (Zhang et al., 2016; Lv et al., 2013; Chen et al., 2020; Jiang et al., 2021). The titanium-containing phase is dispersedly distributed in the blast furnace slag with fine particle size. Thus, no economical and environmentally friendly way to deal with this kind of slag is available to date (Chen et al., 2011; Zheng et al., 2016).

In recent decades, many methods have been developed for the comprehensive utilization of TMC, such as direct reduction (Liu et al., 2014; Sui et al., 2017; Zhou et al., 2019), direct acid leaching (Zhao et al., 2013; Palliyaguru et al., 2020), selective chlorination (Zheng et al., 2017), and low-temperature reduction-water leaching (Zhang et al., 2018). The carbothermal reduction method has obvious advantages in the economic and environmental aspects (Li et al., 2019; Liu et al., 2013; Wang et al., 2020). In this method, iron oxide is reduced to metallic iron by a solid or gas reducing agents in preference to titanium oxide. Then the directly reduced iron and titanium slag separated from reduced products via smelting or magnetic separation. However, the method of recovering titanium from titanium slag is

extremely complicated because of high impurity content and low reactivity. Several studies have prepared iron-based wear-resistant materials from TMC by the carbothermal reduction-nitridation method, in which iron and titanium oxides are reduced to metallic iron and TiC or Ti (C, N), respectively (Wu E, 2016; Zhang et al., 2016). Therefore, the new comprehensive utilization method was proposed in our previous research (Yu et al., 2017). In this method, the TMC was reduced by anthracite to Fe and TiN; then, directly reduced iron and impure TiN were obtained by magnetic separation; finally, pure TiN was prepared from impure TiN through acid leaching. The high value-added TiN was obtained in this process, but the reduction process needed to maintain a high temperature for a long time, which increased the cost.

Several researchers have found that the carbothermal reduction process of iron-containing minerals could be significantly promoted by mechanical activation. In the preparation of rutile or iron-based wear-resistant materials (Fe-TiC or Fe-Ti(C, N) composite materials) by carbothermic reduction of ilmenite, mechanical activation of ilmenite and graphite can observably increase the reaction rate and decrease the onset reaction temperature (Chen et al., 2015; El-Sadek et al., 2013; Pan et al., 2003; Welham, 1996; Y. Chen, 1997). However, the effect of mechanical activation on the reduction of TMC to direct reduced iron and TiN has not been reported.

In the present study, the effect of mechanical activation (referred to as activation hereinafter) on carbothermic reduction and nitridation of titanomagnetite concentrates was investigated by particle size analysis, thermodynamic calculation, thermogravimetric analysis, X-ray diffraction (XRD) analysis, scanning electron microscopy (SEM), and energy-dispersive spectroscopy (EDS) analysis. The possible mechanisms were also discussed.

2. Materials and methods

2.1. Materials

The TMC was obtained from Panzhihua, Sichuan Province, China, and it was subjected to a series of properties analyses. Fig. 1(b) and Table 1 are XRD results and the compositions of TMC, respectively. The SEM images and EDS results are shown in Fig. 2 and Table 2, respectively. Notably, the mineral compositions of TMC are mainly titanomagnetite, magnetite, and ilmenite, and V were doped in the first two phases. The anthracite was used as a reductant in this work, and its chemical compositions are presented in Table 3.

Table 1. Chemical compositions of TMC (mass fraction, %)

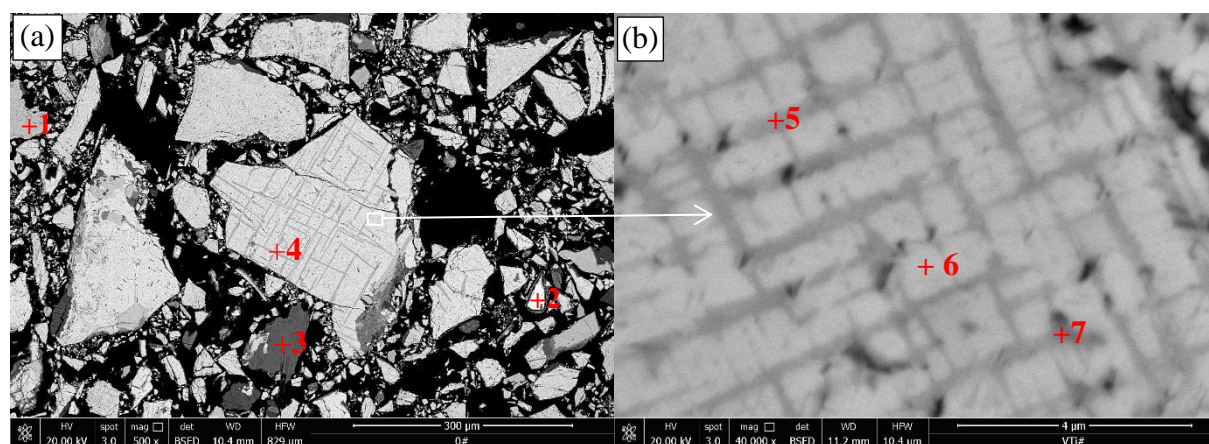| Fe	TiO_2	V_2O_5	Al_2O_3	MgO	SiO_2	CaO	S
56.7	10.5	0.6	2.6	3.0	3.5	0.4	0.6

Fig. 2. Microstructure and EDS results of TMC: (a) typical SEM image; (b) partially enlarged view of (a), where "+" refers to the analyzed point through EDS, and numbers refer to the composition data in Table 2

Table 2. The elemental composition of points showed in Fig. 1 (mass fraction, %)

Point	O	Fe	Ti	V	Mg	Al	Mn	Si	Ca	Na	Phase
1	36.81	28.03	31.87	-	3.30-	1.70	0.95	-	-	-	Ilmenite
2	31.56	65.91	1.87	0.36	-	0.30	-	-	-	-	Magnetite
3	46.44	6.59	1.47	-	9.89-	7.43	-	16.15	9.95	2.07	Silicate
4	36.55	29.34	29.50	-	2.72	0.88	1.01	-	-	-	Ilmenite
5	32.66	49.42	15.42	0.22	2.27	-	-	-	-	-	Titanomagnetite
6	31.83	60.10	7.92	0.16	-	-	-	-	-	-	Titanomagnetite
7	34.93	38.28	17.75	0.41	3.98	4.65	-	-	-	-	Titanomagnetite

2.2. Methods

130.0 g TMC and 33.8 g anthracite (the amount of addition has been determined in our previous studies) were placed into a stainless-steel tank. The planetary four-barrel mill (XPM-Ø100×4, Wuhan Exploration Machinery Factory, China) ran at a rotation speed of 300 rpm for 30, 60, 90, and 120 min, respectively. The four samples above and inactivated samples were added with 0.5 mass % sodium carboxymethyl cellulose and nearly 30 mass% water, respectively; this procedure was followed by homogeneous mixing. The pellets with a diameter ranging from 6 mm to 8 mm were prepared by hands and then dried for 2 h at 120 ℃ in an oven; Thereafter, the pellets were placed into a graphite clay crucible and sealed with a graphite cover and then roasted in a muffle furnace at a constant temperature for a certain period.

The influence of the activation time on the reduction behavior of TMC was investigated. For this purpose, the mass loss behavior of the all samples was analyzed with the thermogravimetry (TG) and derivative thermogravimetry (DTG) method in a thermogravimetric analyzer (HQT-4, Beijing Hengjiu Experimental Equipment, China). Under the condition of a constant N_2 gas flow of 120 ml·min⁻¹ with a heating rate of 25 ℃·min⁻¹, the obtained data are processed using the following formula.

$$TG = \frac{\text{Lost weight}}{\text{Total weight of sample}} \times 100\%$$

$$DTG = \frac{d(TG)}{dT}$$

TG is mass loss of the sample (mass%), DTG is differential of sample mass loss percentage to temperature (%), T is temperature (℃)

2.3. Characterization

The particle size distribution of the samples before and after activation were revealed by a laser diffractometer (Malvern Mastersizer 2000, Malvern, UK). All samples were separately dispersed in absolute ethanol in an ultrasonic bath for 10 min to prevent particle agglomeration.

The phase compositions of the samples were obtained from XRD pattern analysis using an X-ray diffractometer (DX-2700, Hao Yuan Instrument, China) with a 2θ angle ranging from 5 to 80. The morphological and micro-zone chemical composition analysis of the samples were performed by SEM and EDS (MLA650F, FEI, Hillsboro, OR, USA).

3.   Results and discussion

3.1. Analysis of samples after activation

The results of the particle size analysis are shown in Fig. 1(a) d_{50} (the cumulative frequency is 50% at this particle size) is 13.30 μm for the inactivated samples. After activation for 30, 60, 90, and 120 min, d_{50} decrease to 7.37, 5.50, 4.87, and 4.27 μm, respectively. This finding indicates that the particle size drops rapidly in the initial activation stage, and then stabilizes with the increase in activation time. Interestingly, the content of the particles with size between 30 and 160 μm increases after the activation time exceeds 60 min, which may be caused by the re-agglomerates of fine particles. By contrast, the crystal phase of the samples insignificantly changes after activation, as shown in Fig. 1(b).
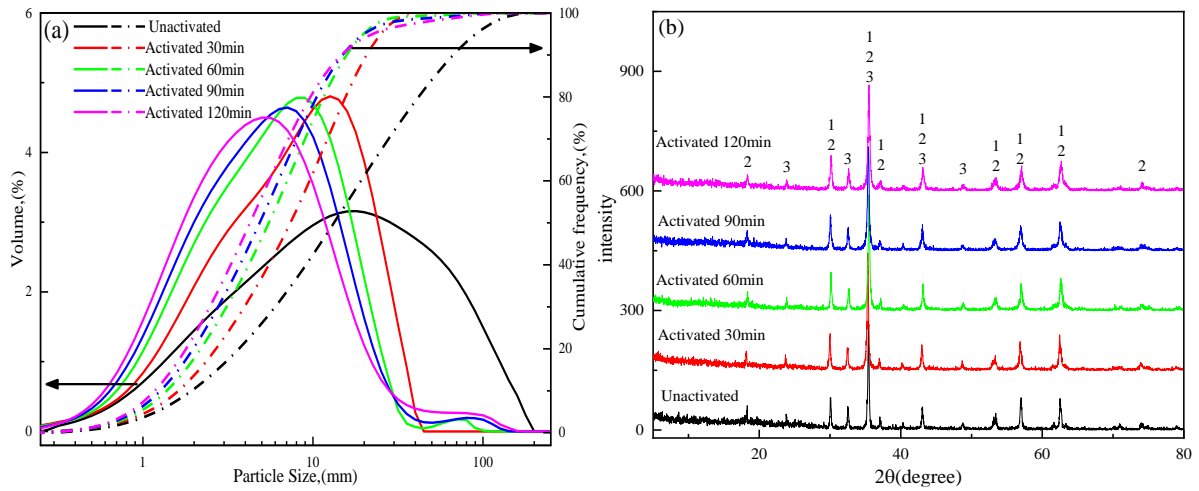
Fig. 1. (a) Particle size distribution as a function of activation time, (b) XRD patterns of the unactivated and activated samples (1-$Fe_{2.75}Ti_{0.25}O_4$; 2-Fe_3O_4; 3-$FeTiO_3$)

3.2. Thermodynamic calculation

According to reports (Hu et al., 2013; Paunova, 2002b; Yu et al., 2017; Yu et al., 2019; Zhang et al., 2016), the reactions that may occur during the carbothermal reduction and nitridation of TMC are as follows:
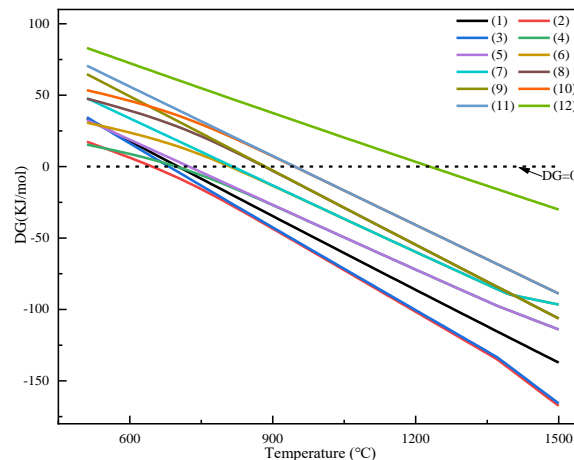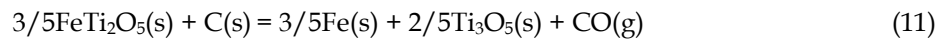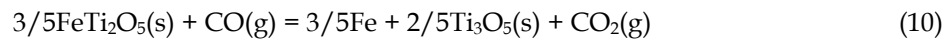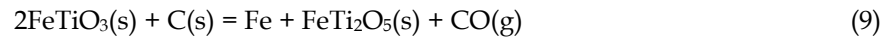
$$C(s) + CO_2(g) = 2CO(g) \tag{1}$$

$$Fe_3O_4(s) + CO(g) = 3FeO + CO_2(g) \tag{2}$$

$$Fe_3O_4(s) + C(s) = 3FeO + CO(g) \tag{3}$$

$$FeO(s) + CO(g) = Fe + CO_2(g) \tag{4}$$

$$FeO(s) + C(s) = Fe + CO(g) \tag{5}$$

$$Fe_2TiO_4(s) + CO(g) = Fe + FeTiO_3(s) + CO_2(g) \tag{6}$$

$$Fe_2TiO_4(s) + C(s) = Fe + FeTiO_3(s) + CO(g) \tag{7}$$

$$2FeTiO_3(s) + CO(g) = Fe + FeTi_2O_5(s) + CO_2(g) \tag{8}$$

$$2FeTiO_3(s) + C(s) = Fe + FeTi_2O_5(s) + CO(g) \tag{9}$$

$$3/5FeTi_2O_5(s) + CO(g) = 3/5Fe + 2/5Ti_3O_5(s) + CO_2(g) \tag{10}$$

$$3/5FeTi_2O_5(s) + C(s) = 3/5Fe(s) + 2/5Ti_3O_5(s) + CO(g) \tag{11}$$

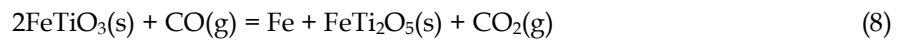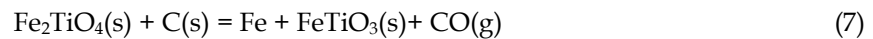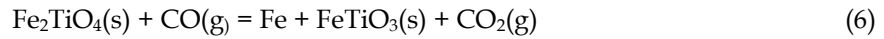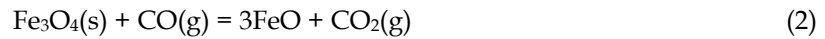$$1/5Ti_3O_5(s) + C(s) + 3/10N_2(g) = 3/5TiN(s) + CO(g) \tag{12}$$

Fig. 3. Gibbs free energy changes for each reaction

With the assumption that Eq. (1) reached equilibrium in the temperature range of 500-1500 °C, the Gibbs free energy changes (ΔG, kJ·mol⁻¹) of these reactions were calculated using Fact-Web (Bale et al.,

2021). Plots of ΔG against temperature are presented in Fig. 4. Standard Gibbs free energy changes instead of ΔG of Eq. (12) and (13) were provided given that the reaction equilibrium constant cannot be calculated.

Fig. 3 shows that ΔG of all reactions decreases with the increase in temperature, and the reaction of Fe_3O_4 reduced to Fe (reactions 2-5) occurs first. Then, Fe_2TiO_4 is reduced to Fe and $FeTiO_3$ (reactions 6, and 7). Subsequently, $FeTiO_3$ is reduced to Ti_3O_5 (reactions 8-11). Finally, Ti_3O_5 is reduced to TiN (reaction 12).

3.3. TG and DTG analysis

Fig. 4 displays the thermogravimetric results of samples activated at different times. Fig. 5(b), reveals three apparent peaks in the DTG curve, from which four stages of mass loss can be observed. The temperature range and the percentage of mass loss of each stage are shown in Table 3.

In the first stage, the mass loss is less than 3%. The release of the volatiles in the anthracite and the slow reduction in TMC are the major reasons for the mass loss in this stage.

During the second stage, ΔTG is between 19.5% and 20.5%. Mass loss of samples at this stage is due to the production of CO and CO_2 gas from reactions 1–7. In general, the reduction reaction is dominated by gas-solid reaction (reactions 2, 4, and 6), and the rate of these reactions is controlled by the gasification rate of coal (reaction 1) (Kim et al., 2002; Otsuka et al., 1962). As the activation time increases, the onset and ending temperatures of this stage are observably decreased. Moreover, the mass loss rate increases significantly. This result implies that the reaction rate at this stage is accelerated by sample activation. Some researchers attribute this finding to the increased solid-solid reaction between TMC and anthracite (Ashrafzadeh et al., 2015; Chen et al., 2015). Furthermore, gasification reaction of carbon (reaction 1) is improved by the decrease in the particle size of anthracite (Jung, 2014).
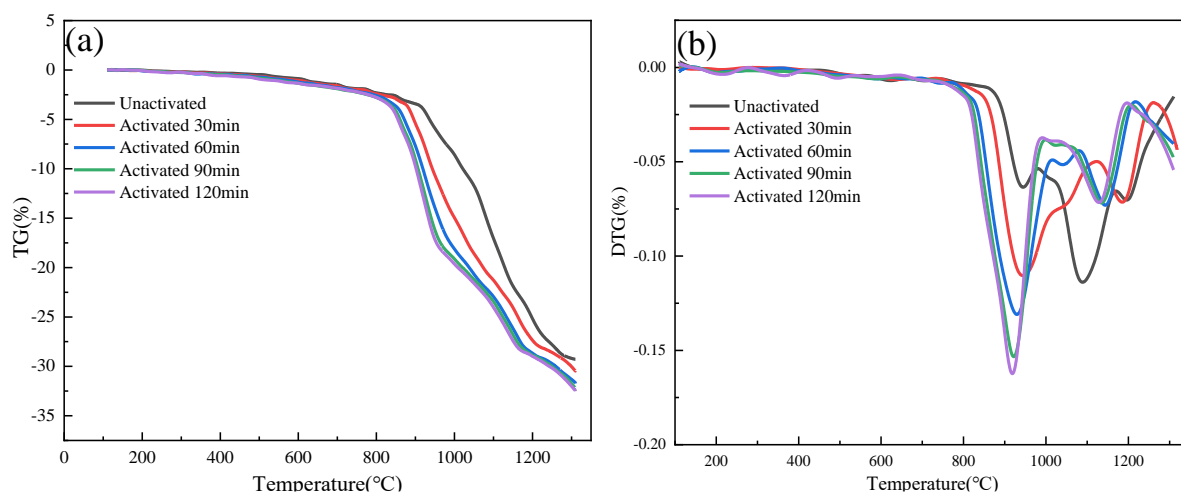

Fig. 4. Thermogravimetric results of samples with different activation times

Table 3. Temperature range and a weight loss percentage at each stage of sample reduction process

Time/min	First stage		Second stage		The third stage		The fourth stage	
	T/°C	ΔTG/%	T/°C	ΔTG/%	T/°C	ΔTG/%	T/°C	ΔTG/%
0	110-850	2.646	850-1165	20.147	1165-1300	6.398		
30	110-800	2.416	800-1120	19.943	1120-1260	6.460	1260-1300	1.205
60	110-775	2.330	775-1080	19.729	1080-1215	6.975	1215-1300	2.283
90	110-750	2.248	750-1065	19.549	1065-1205	7.158	1205-1300	2.765
120	110-750	2.215	750-1050	19.643	1050-1200	7.118	1200-1300	3.026

At the third stage, ΔTG range from 6.35% to 7.20%. The results of thermodynamic calculations in Fig. 3 also indicate that ilmenite is more thermodynamically difficult to be reduced than iron oxides, because it requires higher $P_{co}/(P_{co}+P_{co_2})$ ratio (Hu et al., 2013; Zhou et al., 2019). Thus, the conversion of ilmenite to Ti_3O_5 may occur mainly at this stage (reactions 8-11). Meanwhile, as the activation time increased from 0 min to 120 min, no significant difference is discovered for the maximum rate of mass loss, but the temperature required to reach the maximum rate of mass loss was reduced from 1196 °C to 1128 °C.

During the fourth stage, the mass loss rate of the sample increases slowly with the increase in activation time. The results of the thermodynamic calculation also show that the Ti_3O_5 may convert to TiN at this stage. Furthermore, the decrease in the onset temperature can be clearly observed with increased activation time at this stage. These results indicate that the transformation of Ti_3O_5 to TiN can be improved by sample activation. When the temperature rises to 1300 °C, the mass loss of all samples is unstable, which implies that the reaction is incomplete at this temperature.
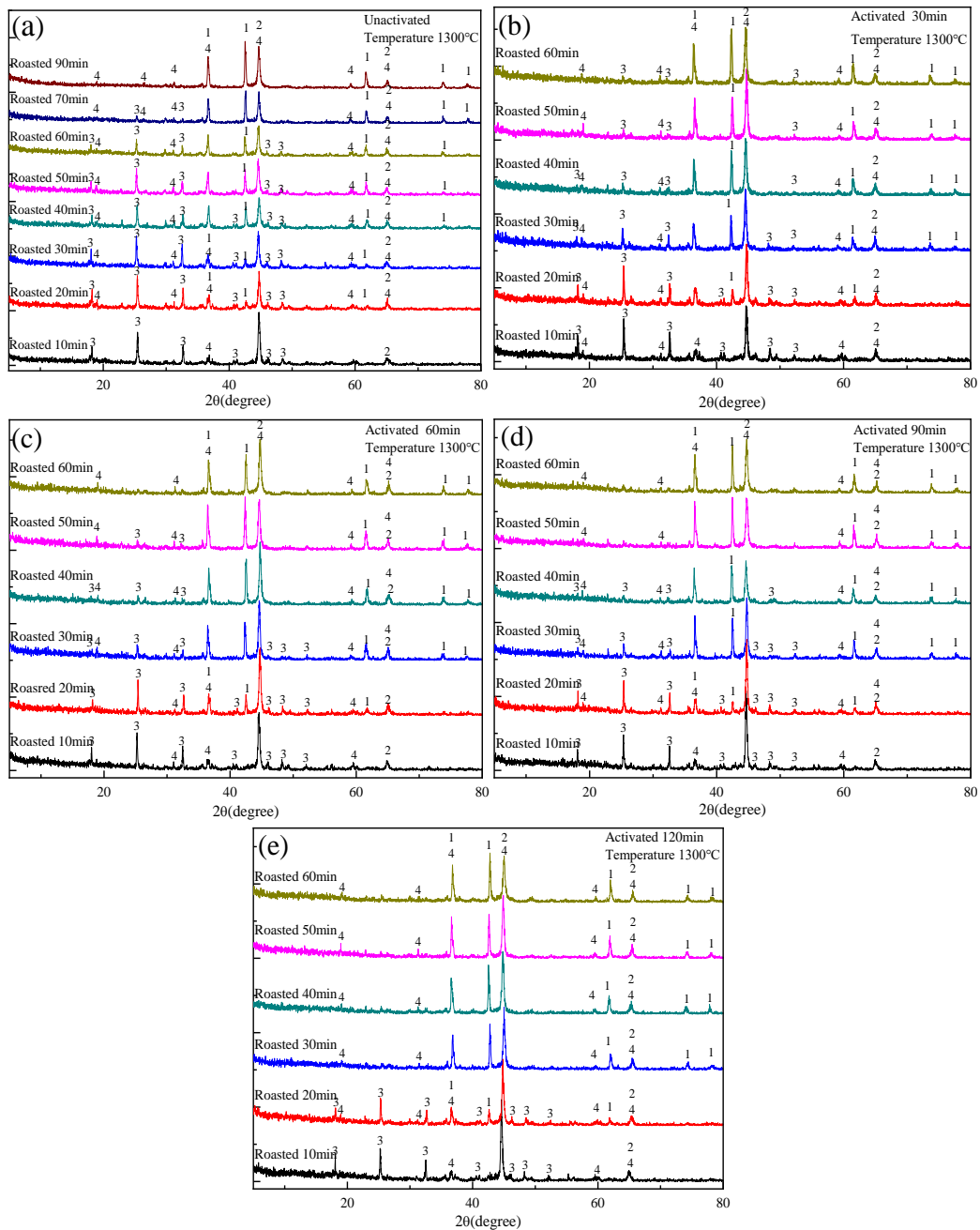
1-TiN, 2-Fe, 3-M_3O_5($MgTi_2O_5$, $FeTi_2O_5$, Ti_3O_5), 4-$MgAl_2O_4$

Fig. 5. XRD results of samples roasted at 1300 °C for different time

3.4. XRD analysis of the roasted products

The effect of samples activation on phase evolution during their reduction was investigated by XRD, and the results as shown in Figs. 5 and 6.

XRD results of unactivated and activated samples roasted at 1300 °C for different times are shown in Fig. 5. According to Fig. 5(a), when the sample is not activated, Fe, M_3O_5, and $MgAl_2O_4$ are observed in the roasted product of roasting for 10 min. M_3O_5 ($MgTi_2O_5$, $FeTi_2O_5$, Ti_3O_5) is considered to be an important precursor for the conversion of titanium oxide to TiN. The peak of TiN is first detected in the product of roasting for 20 min. Then, its intensity increases with the extension of the roasting time. The peak of M_3O_5 is not detected in the product of roasting for 90 min. This finding means that the rate of reduction from iron and titanium oxides to metallic iron and M_3O_5 is very quick, but the rate of conversion from M_3O_5 to TiN is very slow. Thus, this stage is considered the speed-limiting step of TMC reduction into TiN.

Fig. 5(b) demonstrates that, when the sample is activated for 30 min, only a low peak intensity of M_3O_5 is observed in the product of roasting for 60 min. As the activation time increases to 60, 90, and 120 min, the roasting times required for the complete disappearance of the peak of M_3O_5 are 50, 40, and 30 min, respectively, as shown in Figs. 5(c), (d), and (e). This result proves that activation can shorten the time required for TMC to be completely reduced to TiN. Furthermore, the spinel ($MgAl_2O_4$) is found in all the products and has little effect on the reduction system, so it is not discussed in this paper.

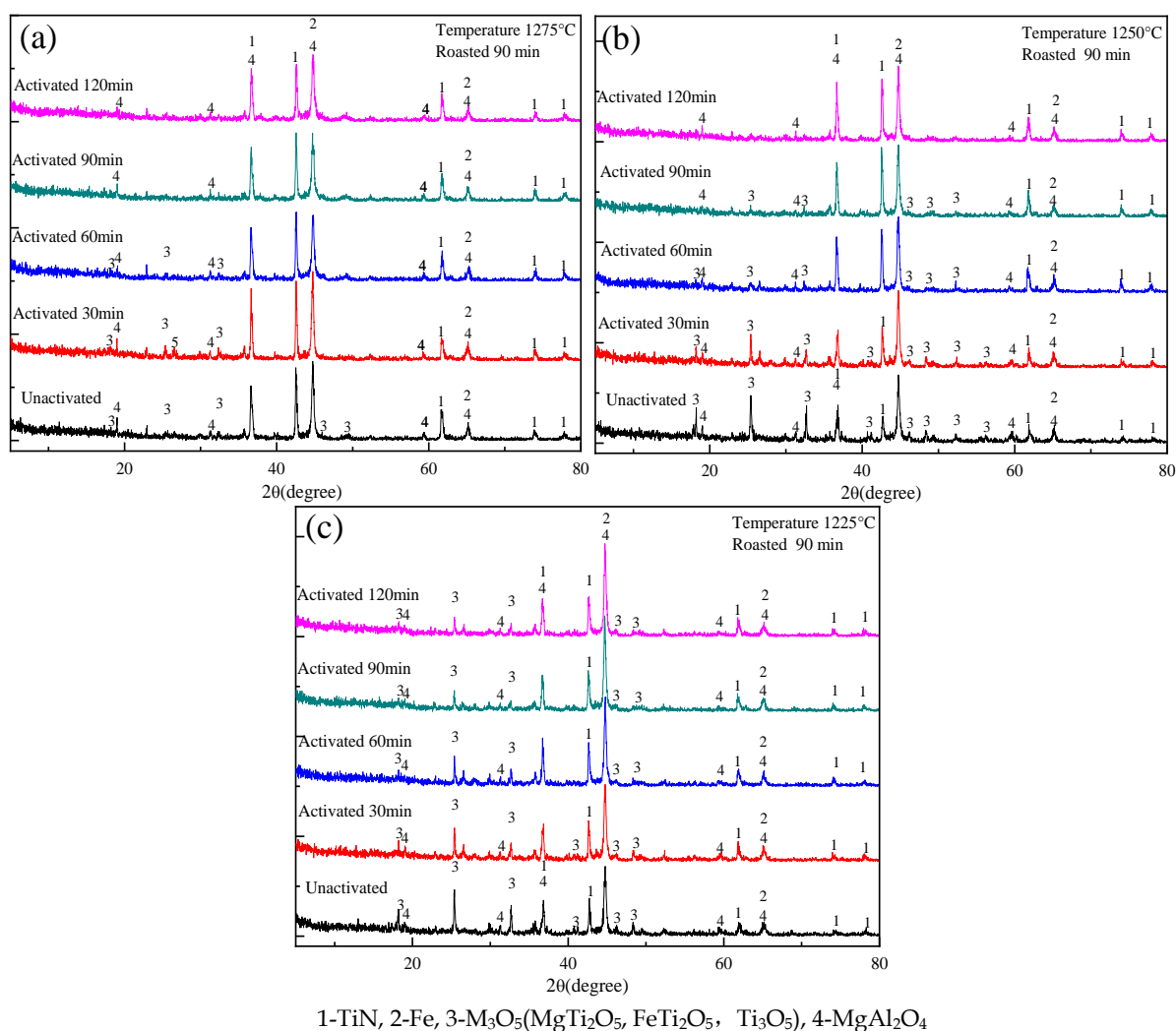1-TiN, 2-Fe, 3-M_3O_5($MgTi_2O_5$, $FeTi_2O_5$, Ti_3O_5), 4-$MgAl_2O_4$

Fig. 6. XRD results of five samples roasted at different temperatures for 90 min

Fig. 6 shows the XRD results of inactivated and activated samples roasted at different temperatures for 90 min. Fig. 6 shows that, when the sample is not activated, M_3O_5 is detected in the roasted products

of roasted at 1225 °C, 1250 °C, and 1275 °C. When samples are activated for 90 and 120 min, the temperatures required to completely convert Ti_3O_5 to TiN decrease to 1250 °C and 1275 °C, respectively. This result indicates that activation of the sample can decrease the temperature required for TMC to be completely reduced to TiN.

From the abovementioned discussion, the reduction process of TMC to TiN can be divided into two stages. The first stage is the reduction of iron and titanium oxides to metallic iron and M_3O_5. This stage is completed very quickly. Thus, the influence of the activation of the sample on this stage not obvious. The second stage is the transformation of M_3O_5 to TiN. This stage is the rate-limiting step in the entire process and can be promoted by activation.
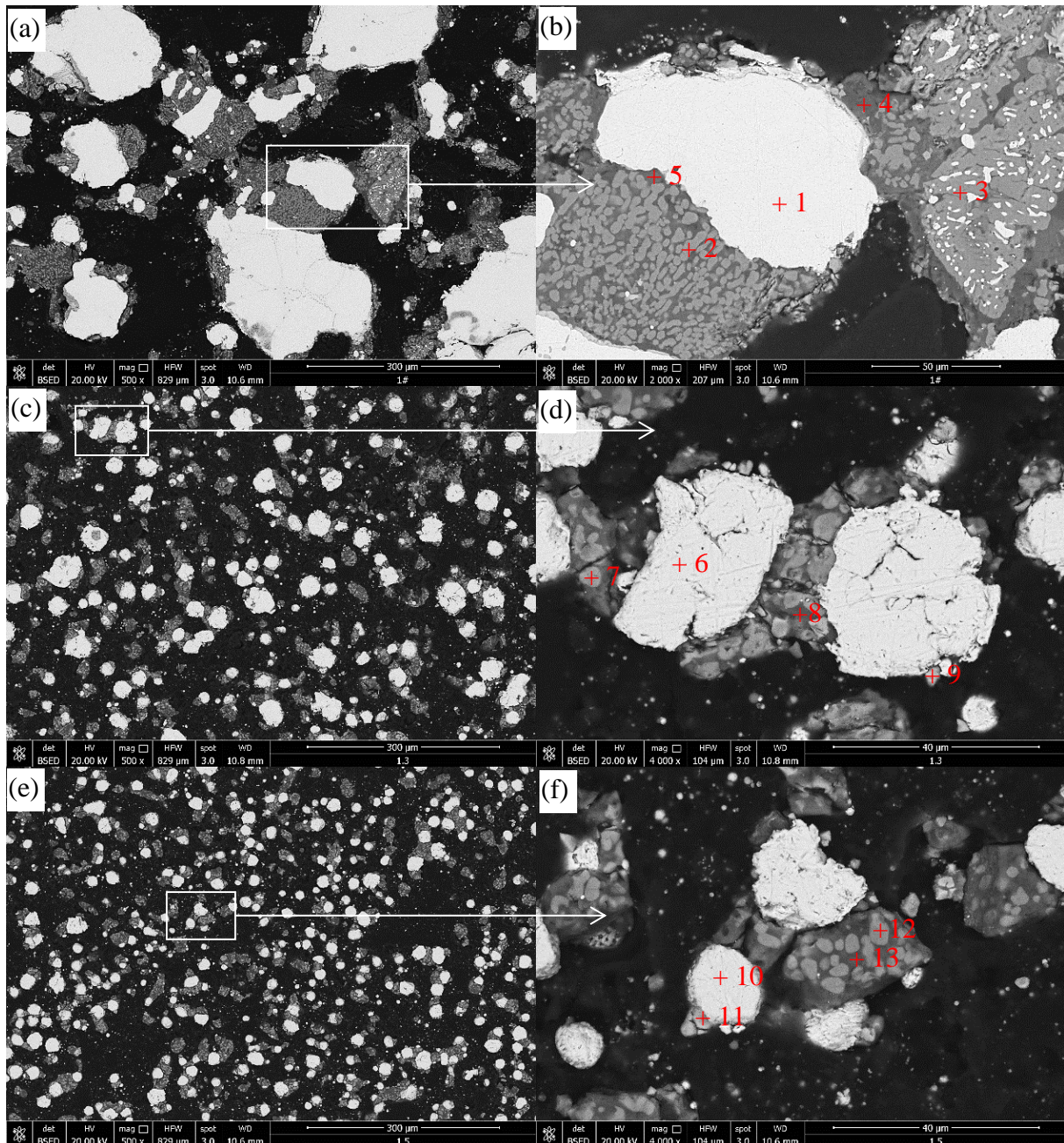

Fig. 7. SEM images of the products obtained from unactivated and activated samples roasting at 1300 °C for 10 min: (a), (b) unactivated; (c), (d) activated 60 min; (e), (f) activated 120 min

3.5. SEM and EDS analysis of the roasted products

Some roasted products were selected for SEM and EDS analyses. to explore the mechanism of mechanical activation accelerating the reduction and nitridation of M_3O_5 to TiN.

Fig. 7 and Table 4 show the SEM images and EDS results of the roasted products, respectively. These roasted products were obtained by roasting the samples without activation and activation for 60 and 120 min at 1300 °C for 10 min. The XRD results presented in Fig. 5 also show that the white particles (points 1, 6, and 10) are the metallic iron, the irregular polygonal gray-white particles (points 9 and 11) are the TiN, the gray particles (points 2, 3, 7, and 12) with smooth curved surfaces are the M_3O_5, and the dark gray area (points 4, 5, 8, and 13) is the impurity phase.

Table 4. Chemical composition of points indicated in Fig. 7. (mass fraction, %)

Point	C	N	O	Mg	Al	Si	S	Ca	Ti	V	Fe	Phase
1	4.31					0.40			0.20		95.09	Fe
2	2.89		39.03	3.62	2.34	0.37		0.46	49.76	0.21	1.32	M_3O_5
3	2.87		38.91	4.94					50.66		2.62	M_3O_5
4	2.69		42.02	16.86	11.05	23.72		1.37	1.63		0.66	Slag
5	1.18		41.83	4.33	12.26	23.72	1.05	10.48	4.48		0.67	Slag
6	5.38					0.77			0.36		93.49	Fe
7	4.81		38.90	2.56	1.81	1.12			49.35	0.30	0.74	M_3O_5
8	4.96		49.02	5.72	13.53	15.17	1.19	8.48	0.86		1.07	Slag
9	6.51	17.05							70.41	5.37	0.66	TiN
10	4.29					0.81			0.29		94.61	Fe
11	3.93	19.89							70.94	3.72	1.32	TiN
12	2.46		39.10	2.95	1.59	0.20			52.85		0.85	M_3O_5
13	5.28		48.19	17.65	6.68	15.54	0.32	3.91	1.73		0.70	Slag

Fig. 7(a) shows the chunks of Fe particles distributed in the roasted products when the sample is unactivated, most of which have a diameter of above 100 µm, and seriously sintered impurity phase and M_3O_5. Two different morphologies of M_3O_5 are observed in Fig. 7(b). The first type of M_3O_5 is distributed on the lower left of figure, it has a particle diameter of several microns, and contains 0.21 mass % V (point 2). Another kind of M_3O_5 is located in on the right side of the figure, and it has a diameter of tens microns, and does not contain V (point 3). The distribution of V element in the samples before and after roasting, reveals that the former M_3O_5 is derived from the reduction in titanomagnetite, and the latter M_3O_5 is due to the reduction in ilmenite. Both M_3O_5 are sintered with impurities to form a dense structure. M_3O_5 is reportedly reduced by C to TiN, and the diffusion rate of C to the surface of M_3O_5 is the rate-determining step (Gou et al., 2017; Welham et al., 1998). Ti_3O_5 in these dense structures has difficulty contacting to C, which prevents Ti_3O_5 from being reduced to TiN.

Table 5. Chemical composition of points indicated in Fig. 8. (mass fraction, %)

Point	C	N	O	Mg	Al	Si	Ca	S	Ti	V	Fe	Phase
1	4.52					0.21					95.27	Fe
2	5.59	26.70				0.24	0.17		62.54	3.60	4.11	TiN
3	4.28	25.13							67.80	1.36	1.43	TiN
4	2.05		36.49	3.33	0.86				49.92		7.35	M_3O_5
5	3.67		47.70	10.11	10.77	14.54	8.99	0.78	3.04		0.40	Slag
6	6.24					0.32			0.54		92.89	Fe
7	3.28	21.33							70.46	4.00	0.93	TiN
8	4.19		45.08	21.97	8.26	16.47	3.70	0.30	1.08		0.57	Slag

Fig. 7(c) shows that, when the activation time is 60 min, the iron particles are mostly between 20 and 40 µm in diameters in the roasted products, and the sintering degrees of M_3O_5 and impurity decrease obviously. As shown in Fig. 7(e), iron particle size is decreased to less than 20 µm, and the sintering degrees of the M_3O_5 and impurity phase are known further mitigated in the roasted products as activation times prolongs to 120 min. Anthracite particles are known to be more fragile than TMC. Thus, the former is being broken into finer particles than the latter, and the latter is wrapped during the activation process. Thus, the sintering between particles is prevented by anthracite in the roasting

process (Yuki Tanaka, 2011). This condition promotes the conversion of M_3O_5 to TiN by increasing the contact area between C and M_3O_5.

On the other hand, the chunks of M_3O_5 was not observed in the roasted products of activated samples as shown in Fig. 7 (c) and (e), this is due to that ilmenite was broken into smaller particles during activation process, and the resulting fine M_3O_5 particles are more easily reduced to TiN. Moreover, Gou, H. et al. (2017) proposed that the metallic iron is an important medium for delivering C to M_3O_5. The contact area of Fe with C and M_3O_5 were increased by decreasing of Fe particle size, this accelerates conversion of M_3O_5 to TiN by enhancing the carburization of iron. Fig. 8(d) and (f) shows that TiN (points 9, 11) was first found in the surface of Fe, which supports the above-mentioned mechanism. The peak of TiN was not detected in the XRD in Fig. 6(c) and (e), which may be because the amount of TiN is too small to be detected by XRD.

Fig. 8 and Table 5 display the SEM image and EDS results of the products obtained from unactivated and activated samples under roasting at 1250 °C for 60 min. Fig. 8(a) and (b) reveal that TiN and two kinds of M_3O_5 was found in the roasted product without activation. However, M_3O_5 is not observed in the roasted product after 120 min of activation, as shown in Figs. 8(c) and (d). This result also proves that the transformation of M_3O_5 to TiN is promoted through the activation of the sample.
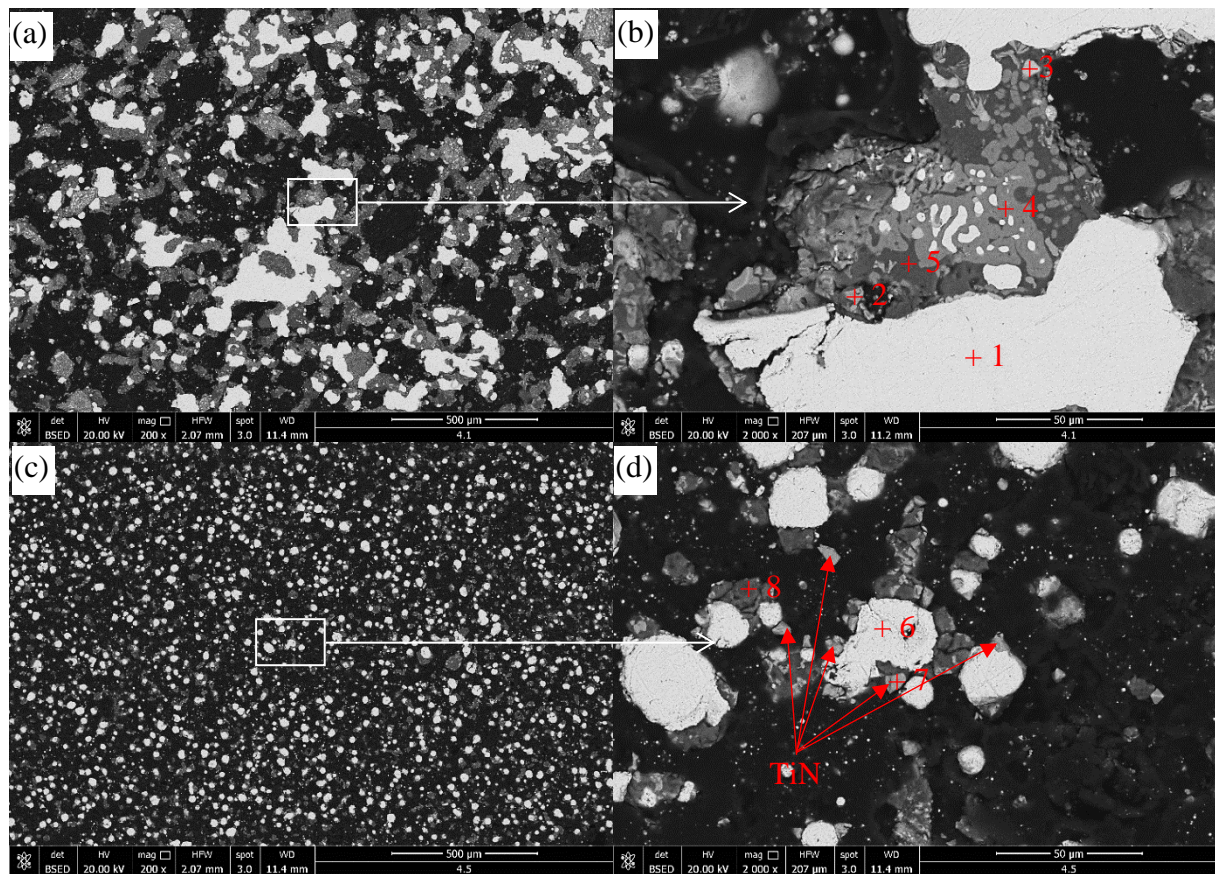

Fig. 8. SEM images of the products roasting at 1250 °C for 60 min: (a), (b) unactivated; (c), (d) activated 120 min

4. Conclusions

The effect of mechanical activation on carbothermic reduction and nitridation of titanomagnetite concentrates was investigated for the first time, which mechanism was discussed in detail. The major conclusions are drawn as follows. The reduction and nitridation of TMC could be divided into two stages under constant temperature. The first stage is the reduction in iron and titanium oxides to metallic iron and M_3O_5. The second stage is the reduction and nitridation of M_3O_5 to TiN, which is the rate-limiting step for the entire process. Two reasons have been found to hinder the conversion of M_3O_5 to TiN by impeding the transfer of carbon to the M_3O_5 surface: firstly, M_3O_5 were severely sintered with impurities to form a dense structure. It's worth noting that the chunks and thin of M_3O_5 well formed by

reducing ilmenite and titanomagnetite, respectively, and the former is more difficult to convert to TiN than the latter; secondly, Iron as a medium for delivering C to M_3O_5 had a diameter of more than 100 μm. The conversion of M_3O_5 to TiN were promoted by activation of sample, because with the extension of the activation time of the sample, the sintering degrees of the impurity and M_3O_5 were mitigated. The size of the iron particles was also decreased, which enhanced the diffusion of C to the surface of M_3O_5. Meanwhile, the bulk of ilmenite was broken in the activation process, which prevented the formation of chunks of M_3O_5.

There will be further study on the influence of mechanical activation on the sintering phenomenon in the reduction process of titanomagnetite concentrate, which has rarely been reported. In addition, the difference in the reduction behavior of ilmenite and titanomagnetite in titanomagnetite concentrates deserves further attention.

Acknowledgments

References

ASHRAFZADEH, M, SOLEYMANI, AP, PANJEPOUR, M, SHAMANIAN, M, 2015. *Cementite Formation from Hematite–Graphite Mixture by Simultaneous Thermal–Mechanical Activation*. Metallurgical and Materials Transactions B. 46 (2), 813-823.

BALE, C.W., BELISLE, E. *Fact-Web Suite of Interactive Programs*. Available online: www.factsage.com (accessed on 21 March 2021).

CHEN, D, SONG, B, WANG, L, QI, T, WANG, Y, WANG, W, 2011. *Solid State Reduction of Panzhihua Titanomagnetite Concentrates with Pulverized Coal.* Minerals Engineering. 24 (8), 864-869.

CHEN, L, ZHEN, Y, ZHANG, G, CHEN, D, WANG, L, ZHAO, H, MENG, F, QI, T, 2020. *Carbothermic Reduction of Vanadium Titanomagnetite with the Assistance of Sodium Carbonate*. International Journal of Minerals, Metallurgy and Materials. DOI: 10.1007/s12613-020-2160-7

CHEN, M, TANG, A, XIAO, X, 2015. *Effect of Milling Time on Carbothermic Reduction of Ilmenite*. Transactions of Nonferrous Metals Society of China. 25 (12), 4201-4206.

EL-SADEK, MH, MORSI, MB, EL-BARAWY, K, EL-DIDAMONY, HA, 2013. *Mechanochemical Synthesis of Fe–TiC Composite from Egyptian Ilmenite Ore*. International Journal of Mineral Processing. 120, 39-42.

GOU, H, ZHANG, G, HU, X, CHOU, K, 2017. *Kinetic Study on Carbothermic Reduction of Ilmenite with Activated Carbon*. Transactions of Nonferrous Metals Society of China. 27 (8), 1856-1861.

HU, T, LV, X, BAI, C, LUN, Z, QIU, G, 2013. *Reduction Behavior of Panzhihua Titanomagnetite Concentrates with Coal*. Metallurgical and Materials Transactions B. 44 (2), 252-260.

JIANG, T, XU, L, ZHONG, Q, LIU, C, LIU, H, RAO, M, PENG, Z, LI, G, 2021. *Efficient Preparation of Blast Furnace Burdens from Titanomagnetite Concentrate by Composite Agglomeration Process*. JOM. 73 (1), 326-333.

JUNG, S, 2014. *Effects of the Content and Particle Size of Char in the Composite on the Carbothermic Reduction of Titanomagnetite at 1100°C*. ISIJ International. 54 (12), 2933-2935.

KIM, JJ, CHOI, Y, SURESH, S, ARGON, AS, 2002. *Nanocrystallization During Nanoindentation of a Bulk Amorphous Metal Alloy at Room Temperature*. Science. 295 (5555), 654-7.

LI, W, WANG, N, FU, G, CHU, M, ZHU, M, 2017. *Influence of Roasting Characteristics on Gas-Based Direct Reduction Behavior of Hongge Vanadium Titanomagnetite Pellet with Simulated Shaft Furnace Gases*. Powder Technology. 310, 343-350.

LI, X, KOU, J, SUN, T, WU, S, ZHAO, Y, 2019. *Effects of Temperature on Fe and Ti in Carbothermic Reduction of Vanadium Titanomagnetite with Adding MgO*. Physicochemical Problems of Mineral Processing. 55 (4), 917-927.

LIU, C, ZHANG, L, PENG, J, LIU, B, XIA, H, GU, X, SHI, Y, 2013. *Effect of Temperature on Dielectric Property and Microwave Heating Behavior of Low Grade Panzhihua Ilmenite Ore*. Transactions of Nonferrous Metals Society of China. 23 (11), 3462-3469.

LIU, S, GUO, Y, QIU, G, JIANG, T, CHEN, F, 2014. *Solid-State Reduction Kinetics and Mechanism of Pre-Oxidized Vanadium–Titanium Magnetite Concentrate*. Transactions of Nonferrous Metals Society of China. 24 (10), 3372-3377.

LV, X, LUN, Z, YIN, J, BAI, C, 2013. *Carbothermic Reduction of Vanadium Titanomagnetite by Microwave Irradiation and Smelting Behavior*. ISIJ International. 53 (7), 1115-1119.

OTSUKA, K, KUNII, D, 1962. *Reduction of Powdery Ferric Oxide Mixed with Graphite Particles*. J. Chem. Eng. Jpn. 2, 46-50.

PALLIYAGURU, L, KULATHUNGA, US, JAYARATHNA, LI, JAYAWEERA, CD, JAYAWEERA, PM, 2020. *A Simple and Novel Synthetic Route to Prepare Anatase TiO_2 Nanopowders From Natural Ilmenite Via the H_3PO_4/NH_3 Process*. International Journal of Minerals, Metallurgy and Materials. 27 (6), 846-855.

PAN, FS, LI, K, TANG, AT, WANG, Y, ZHANG, J, GUO, ZX, 2003. *Influence of High Energy Ball Milling on the Carbothermic Reduction of Ilmenite*. Materials Science Forum. 437-4, 105-108.

PAUNOVA, R, 2002a. *Thermodynamic Study of the Reduction of Titanium Magnetite Concentrate with Solid Carbon*. Metallurgical and Materials Transactions B. 33 (4), 633-638.

PAUNOVA, R, 2002b. *Thermodynamic Study of the Reduction of Titanium Magnetite Concentrate with Solid Carbon*. Metallurgical and Materials Transactions B. 33 (4), 633-638.

SUI, Y, GUO, Y, JIANG, T, XIE, X, WANG, S, ZHENG, F, 2017. *Gas-Based Reduction of Vanadium Titano-Magnetite Concentrate: Behavior and Mechanisms*. International Journal of Minerals, Metallurgy, and Materials. 24 (1), 10-17.

WANG, X, LI, Z, SUN, T, KOU, J, LI, X, 2020. *Factor Analysis on the Purity of Magnesium Titanate Directly Prepared from Seashore Titanomagnetite Concentrate through Direct Reduction*. International Journal of Minerals, Metallurgy and Materials. 27 (11), 1462.

WELHAM, NJ, 1996. *A Parametric Study of the Mechanically Activated Carbothermic Reduction of Ilmenite*. Minerals Engineering, 9, 1189-1200.

WELHAM, NJ, WILLIS, PE, 1998. *Formation of TiN/TiC-Fe Composites from Ilmenite (FeTiO3) Concentrate*. Metallurgical and Materials Transactions B. 29 (5), 1077-1083.

WU E, ZRYS., 2016. *Preparation of Fe-Ti (C, N) Composites from Titanomagnetite Concentrate by Carbothermal Reduction in Air Atmosphere*, pp. 46-50.

Y, CHEN, 1997. *Ball Milling Assisted Low Temperature Formation of iron-TiC Composite*. Scripta Materialia. 36 (9), 989-993.

YU, W, WEN, X, CHEN, J, KUANG, J, TANG, Q, TIAN, Y, FU, J, HUANG, W, QIU, T, 2017. *Preparation of Direct Reduced Iron and Titanium Nitride from Panzhihua Titanomagnetite Concentrate through Carbothermic Reduction-Magnetic Separation*. Minerals. 7 (11), 220.

YU, W, WEN, X, CHEN, J, TANG, Q, DONG, W, ZHONG, J, 2019. *Effect of Sodium Borate on the Preparation of TiN from Titanomagnetite Concentrates by Carbothermic Reduction–Magnetic Separation and Acid Leaching Process*. Minerals. 9 (11), 675.

YUKI TANAKA, TUKO, 2011. *Reaction Behavior of Coal Rich Composite Iron Ore Hot Briquettes Under Load at High Temperatures Until 1 400°C*. ISIJ International.

ZHANG, G, FENG, K, YUE, H, 2016. *Theoretical Analyses and Experimental Investigations of Selective Carbothermal Reactions of Vanadium-Bearing Titanomagnetite Concentrates for Preparation of Iron-Based Wear-Resistant Material*. JOM. 68 (9), 2525-2532.

ZHANG, Y, WANG, L, CHEN, D, WANG, W, LIU, Y, ZHAO, H, QI, T, 2018. *A Method for Recovery of Iron, Titanium, and Vanadium from Vanadium-Bearing Titanomagnetite*. International Journal of Minerals, Metallurgy, and Materials. 25 (2), 131-144.

ZHAO, L, LIU, Y, WANG, L, ZHAO, H, CHEN, D, ZHONG, B, WANG, J, QI, T, 2013. *Production of Rutile TiO2 Pigment from Titanium Slag Obtained by Hydrochloric Acid Leaching of Vanadium-Bearing Titanomagnetite*. Industrial & Engineering Chemistry Research. 53 (1), 70-77.

ZHAO, W, CHU, M, WANG, H, LIU, Z, TANG, J, YING, Z, 2019. *Reduction Behavior of Vanadium-Titanium Magnetite Carbon Composite Hot Briquette in Blast Furnace Process*. Powder Technology. 342 (214-223.

ZHENG, F, CHEN, F, GUO, Y, JIANG, T, TRAVYANOV, AY, QIU, G, 2016. *Kinetics of Hydrochloric Acid Leaching of Titanium from Titanium-Bearing Electric Furnace Slag*. JOM. 68 (5), 1476-1484.

ZHENG, H, SUN, Y, LU, J, DONG, J, ZHANG, W, SHEN, F, 2017. *Vanadium Extraction from Vanadium-Bearing Titanomagnetite by Selective Chlorination Using Chloride Wastes (FeClx)*. Journal of Central South University. 24 (2), 311-317.

ZHOU, M, JIANG, T, DING, X, MA, S, WEI, G, XUE, X, 2019. *Thermodynamic Study of Direct Reduction of High-Chromium Vanadium–Titanium Magnetite (HCVTM) Based on Phase Equilibrium Calculation Model*. Journal of Thermal Analysis and Calorimetry. 136 (2), 885-892.